Critical current across grain boundaries in melt-textured $YBa_2Cu_3O_{7-\delta}$ rings

H. Claus,[1,2] U. Welp,[1] H. Zheng,[1] L. Chen,[1] A. P. Paulikas,[1] B. W. Veal,[1] K. E. Gray,[1] and G. W. Crabtree[1]
[1]*Materials Science Division, Argonne National Laboratory, Argonne, Illinois 60439-4830*
[2]*Department of Physics, University of Illinois at Chicago, Chicago, Illinois 60607-7059*
(Received 19 January 2001; revised manuscript received 16 April 2001; published 19 September 2001)

We determine the critical current J_{cB} of grain boundaries fabricated by ''welding'' of melt-textured YBCO with various degrees of **ab**-plane misalignment. J_{cB} is determined by monitoring the magnetic moment due to persistent shielding currents, which were induced in rings containing two sections of a single grain boundary. The voltage drop across the junctions is estimated to be below 10^{-12} V, much smaller than in typical transport measurements. As the temperature or magnetic field is increased, an abrupt decrease (kink) is observed in the magnetic moment of the ring when the induced shielding current in the ring exceeds the critical current across the boundaries. The kink signals that flux has begun to penetrate through the grain boundaries into the bore of the ring. This behavior is confirmed by magneto-optical imaging. We observe that grain boundaries with [001] tilt mismatch angles up to 5° have critical current densities in excess of 10^4 A/cm^2, comparable to the bulk current density. At larger mismatch angles, the critical current rapidly decreases with increasing angle. The qualitative behavior of J_{cB} as function of temperature, magnetic field, and misorientation angle is similar to that observed YBCO grain boundaries manufactured by other methods.

DOI: 10.1103/PhysRevB.64.144507 PACS number(s): 74.72.Bk, 74.60.Ge, 74.60.Jg, 74.62.Dh

INTRODUCTION

Recently, it has been demonstrated that bulk melt-textured $YBa_2Cu_3O_{7-\delta}$ (YBCO) components can be artificially joined through a ''welding'' process.[1–10] This technique opens the way for the fabrication of large-scale superconducting devices such as trapped high-field magnets, hysteresis motors, magnetic bearings, and current limiters. The performance of these devices, though, depends crucially on the critical current density that can be passed across the weld joint. Also, for the assembly of large YBCO structures, **ab**-plane misalignment of two adjacent pieces to be welded often cannot be avoided. It is well established that an important factor controlling the critical current density of grain boundaries in thin-film as well as in bulk $YBa_2Cu_3O_{7-\delta}$ is the overall misorientation angle of the grains.[11–18] It is thus important to study the effect of **ab** misalignment across the weld joints on the critical current, which can be passed across the joint.

Here, we report on the field and temperature dependence of the critical current density J_{cB} of artificial [001] tilt boundaries of various misorientations ranging from 0 to 11° that were produced by the welding process. A feature of our measurements is that the critical currents of the grain boundaries are determined with an extremely low-voltage criterion. J_{cB} is determined by monitoring the persistent currents flowing in rings that were patterned across the boundaries. Persistent current measurements are ideally suited for this experiment since they alleviate the need for high-current contacts. At the same time they yield values of the critical current density determined at very low effective voltage, below 10^{-12} V. This low-voltage criterion is similar to that encountered in some of the intended applications such as trapped field magnets and magnetic bearings. Another example where very low-voltage criterion is of importance is the dissipation across grain boundaries (GB's) in textured, coated conductors of $YBa_2Cu_3O_x$ (YBCO) made on IBAD (ion-beam assisted deposition) substrates. In conventional transport methods the voltage criterion is generally 0.1–1 μV over distances of $\sim$1 cm. Since the superconducting layer exhibits grain sizes smaller than 1 micron, there are $\sim 10^4$ GB's/cm of conductor length. Thus, in obtaining J_c from a typical I-V measurement, which is appropriate for determining engineering J_c values, the voltage drop across an individual grain boundary is 10–100 pV. In order to develop coated conductor technology, it is useful to study the properties of individual, isolated grain boundaries under these applications-relevant conditions.

In this paper we demonstrate that the critical current of a single grain boundary, present in a superconducting ring, can be easily detected from an abrupt change in slope (kink) in the diamagnetic magnetization, observed as the temperature or magnetic field is scanned. We find that for misorientation angles up to 5° grain boundaries associated with weld joints carry essentially the same current as the bulk whereas for larger angles a strong suppression of J_{cB} is found. Critical currents of the grain boundaries are determined in magnetic fields between 0 and 2 T.

SAMPLE PREPARATION

Melt-textured cylindrical YBCO monoliths were produced using a top-seeding method. Melt textured Sm123, oriented with its c axis parallel to the cylinder axis, served as the seeding material. Typically, between 10- and 26-mm diameter cylindrical samples were produced. The starting materials were Y123 and Y211 powders (99.9% purity, Superconductive Components) mixed in the ratio of 75:25 by weight containing an added 0.2 wt % of PtO_2. The powders were thoroughly mixed in an agate ball mill and were pressed into cylindrical billets under a pressure of 100 MPa. To eliminate porosity, the billets were heated, in an oxygen atmosphere to 1040 °C, above the decomposition temperature of YBCO, where they were held for 0.5 h and

were then furnace cooled to room temperature.

To texture the samples, these densified billets were then processed in air using the following heating cycle. The sample was first heated to 1030 °C, above the peritectic point, and kept there for 2 h for complete melting. The sample was then fast cooled to 995 °C (undercooled state). To obtain the texturing, the sample was then slow cooled at a rate of 0.5–1 °C/h to 965 °C and subsequently fast cooled (~100°C/h) to room temperature. Processing was done in a vertical tube furnace with a vertical temperature gradient at the sample location of ~4 °C/cm.

The densification step was added to eliminate the extensive porosity which typically appears in melt textured YBCO. This treatment, in an oxygen (nitrogen free) atmosphere, exploits the fast diffusion of oxygen through YBCO and avoids the trapping of nitrogen gas in bubbles within the melt. At the highest temperature in the densification step, the sample has decomposed to a Ba and Cu rich liquid containing dispersed Y211. When such samples are melted in air, a profusion of voids, or bubbles, form within the material. The bubbles, which initially exist in the melt as pockets of entrapped air, persist through the melt texturing process and ultimately appear as voids in the textured solid. However, oxygen has an extremely high diffusivity within YBCO (and, perhaps within the Ba and Cu rich liquid), so it is free to diffuse through the billet as solidification proceeds (or, possibly even before solidification occurs). Thus the oxygen will likely escape entirely from a bubble. However, the nitrogen does not readily diffuse through the material, and hence remains trapped, preserving the bubbles through the melt texturing process. The trapped nitrogen, and hence the voids, can be eliminated by adding a melting step, prior to the texturing step, in an oxygen atmosphere.

The resulting samples were void free, being nearly 100% dense. The melt-textured cylinders were then cut in half with a diamond saw and the two half cylinders were welded back together after slicing off a wedge-shaped piece to create desired misalignment of the **ab**-plane orientation. For the welding agent, we used Ag doped YBCO (75% Y123+25% Y211 with 10% added Ag_2O; all percentages in wt %). This mixture has a melting temperature about 30° lower than undoped YBCO.[9,10] In the welding process, the filler material is heated above its decomposition temperature, but the maximum sample temperature (1000 °C) remains below the decomposition temperature of the YBCO pieces. With cooling (0.5–1 °C/h), the filler material solidifies, and crystallographically oriented growth fronts proceed outward from the misaligned YBCO faces. The growth fronts eventually merge to create the grain boundary. After the welding procedure, the oxygen stoichiometry was fixed by heat treating the sample at 450 °C for 10 days in flowing oxygen. The samples were then sliced perpendicular to the **c** axis into disks about $t=1.1$-mm thick. Rings with outer diameter of $D=5$ mm and inner diameter of $d=3$ mm were then extracted by core drilling across the weld joints.

RESULTS AND DISCUSSION

The use of persistent currents in ring-shaped samples for the evaluation of single crystal, polycrystalline and thin-film YBCO has been described before.[19–21] Here, we extend this technique to the study of isolated grain-boundaries in melt-textured YBCO. A similar approach has recently been used for the study of small angle grain boundaries in RABiTS (rolling assisted bi-axially textured superconductor) coated conductors.[22] Magnetic measurements were performed in a noncommercial low-field superconducting quantum interference device (SQUID) magnetometer in the range of 4–100 K and 0–200 G as well as in a commercial vibrating-sample magnetometer (VSM) (Lake Shore) in the range of 4–100 K and 0–7 T. The distribution of the magnetic fields in the sample was also directly visualized using a high-resolution magneto-optical imaging system.[23]

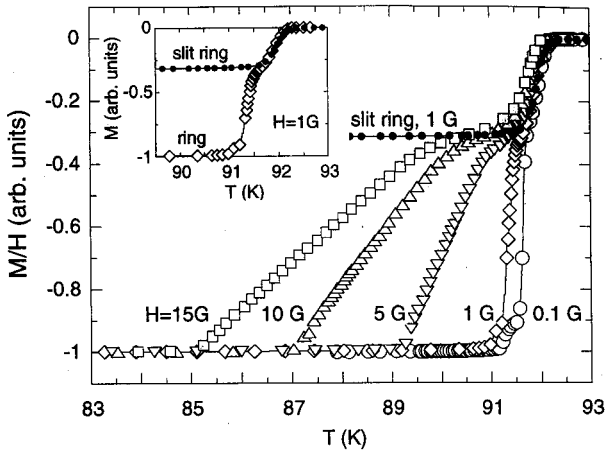

FIG. 1. Magnetic susceptibility M/H of an YBCO ring cut across an [001] tilt grain boundary (weld joint with an 11°-mismatch angle). The ring was initially cooled to low temperatures. A magnetic field as indicated was then applied. The data were taken on warming in constant field. Also shown is the signal obtained after a slit was cut into the ring (see inset).

Low-field measurements (zero-field cooled)

Figure 1 displays SQUID dc magnetization measurements taken from a ring sample after cooling to low temperatures in zero applied field. The ring cuts across a weld joint that contains an 11° [001] tilt boundary. The magnetic field was applied normal to the plane of the ring. The data in Fig. 1 are displayed as magnetic susceptibility M/H, as a function of temperature, for a number of applied magnetic fields. After the ring was cooled to low temperature in zero field, a magnetic field (numbers labeling the curves in Fig. 1) was applied and the sample was warmed at constant magnetic field.

At the lowest temperatures, where M is independent of temperature, flux is completely excluded from the ring bore, either because $H<H_{c1}$ (for both the bulk and the grain boundary; a Meissner state), or because pinning is sufficiently strong, everywhere around the ring, to prevent the flow of flux into the bore of the ring. As the temperature is increased (Fig. 1), the critical current across the GB will fall, and the shielding current circulating around the ring will eventually exceed the critical current across the boundary. At this point flux will begin to leak into the ring, decreasing the

observed magnetization. This onset of flux penetration into the ring produces the abrupt decrease in $M(T)$ that is clearly observed in Fig. 1.

Considering the ring to be a single-turn solenoid, the induced current providing shielding of the ring bore can be estimated from the simple expression $I=D^*H$, where D is the outer diameter of the ring and H is the applied magnetic field. Equivalently, $I(A)=0.4$ H (G). Thus, for a field of 15 G applied at low temperatures (e.g., below 85 K; see Fig. 1), a shielding current of 6 A circulates around the ring. Consequently, at a temperature of 85 K (when flux begins to penetrate into the ring) the critical current across the boundary is 6 A. The analysis presented here is a first approximation to the evaluation of the complex current distribution in the ring.[24] In particular, currents are not only concentrated at the outside circumference but also at the top and bottom surfaces of the ring as is directly seen in the magneto-optical images (see below). As a consequence the currents determined from the above relation are slightly overestimated.[25]

As the temperature is further increased above the kink temperature T_k, the shielding current flowing around the ring becomes limited by the declining critical current across the boundary and flux increasingly leaks through the GB into the bore of the ring. The ring material itself (annulus) is still completely shielded, i.e., part of the shielding current flows parallel to the junction to the inner periphery where it flows in the reverse direction. The nearly linear decrease in M vs T above T_k reflects a nearly linear decrease of J_{cB} with temperature.

The plateau in M/H vs T reached at about 30% of the full shielding signal indicates that the critical current across the junction has dropped to zero. The field inside the bore now almost equals the field outside and the current at the inner periphery equals the current on the outer periphery. The remaining signal is due to flux expulsion from the annulus, which has a transition temperature of about 92 K. The plateau in $M(T)$ coincides with the diamagnetic signal from the ring after a slit has been cut into the ring to prevent any circulating shielding currents. The inset of Fig. 1 compares the signal of the ring at 1 G, before and after the slit was cut.

It is instructive to subtract the magnetization of the slit ring (annulus) from the total signal of Fig. 1. This is done in Fig. 2 which displays the difference $M_{\text{ring}}-M_{\text{slit ring}}$ as a function of temperature. The numbers labeling the curves are the magnetic-field values. As mentioned above, the nearly linear decreasing magnetization curves are determined by the decrease of the critical current across the junction as the temperature is increased. As expected the curves for the different fields are essentially parallel, determined by the decrease in $J_{cB}(T)$. The higher the magnetic field the larger is the induced shielding current in the ring, i.e., the lower the temperature at which $J_{cB}(T)$ starts limiting the shielding current around the ring. However, the curves are slightly displaced, being nearly parallel on the temperature axis, i.e., the higher the applied field the lower the temperature at which $J_{cB}(T)$ reaches zero. This field-dependent shift in $M(T)$ is due to the increasing average field inside the junction (see discussion below about the field dependence of the critical current).

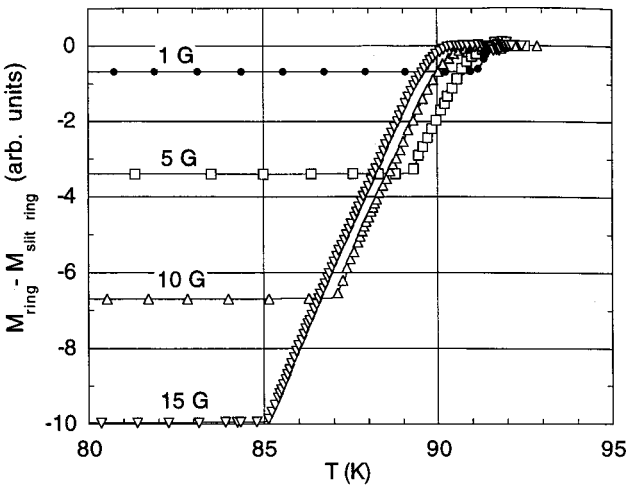

FIG. 2. Magnetic moment of the ring (of Fig. 1) minus the moment of the slit ring as a function of temperature. The numbers labeling the curves are the magnetic-field values in G.

An alternative procedure to determine the critical current across the grain boundary is from an evaluation of the low-field $M(H)$ curves, obtained from VSM measurements. The ring was initially cooled in zero field to a predetermined temperature. Then the field was increased at a constant rate of 1.5 G/s and the magnetization recorded at constant temperature. Figure 3 displays the results for a series of $M(H)$ scans recorded between 0 and 250 G, after cooling to the indicated temperatures, for the same ring as used in Fig. 1. For each scan, a well-defined kink is observed in $M(H)$, reminiscent of the kink behavior observed in Fig. 1 for $M(T)$. The initial slope of $M(H)$ is determined by the shape of the ring (demagnetization factor) and is independent of temperature. It corresponds to complete flux exclusion from the ring (Meissner state). The experimental value for the demagnetization factor determined from the slope of M vs H,

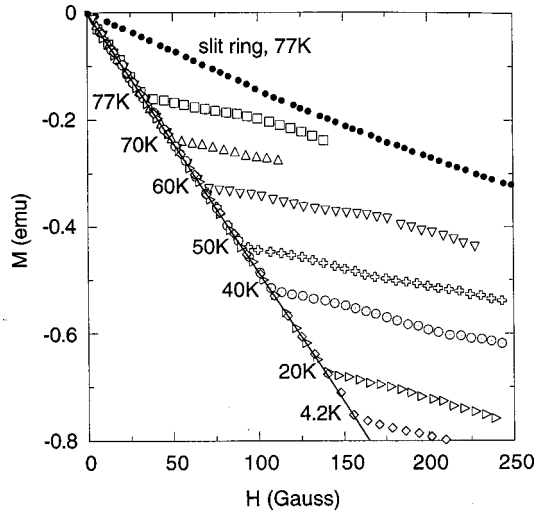

FIG. 3. Magnetic moment of the ring used for Fig. 1 vs magnetic field at various temperatures as indicated. The data were taken after initially cooling in zero field from above T_c to the temperature of measurement. Also shown is the magnetization of the slit ring.

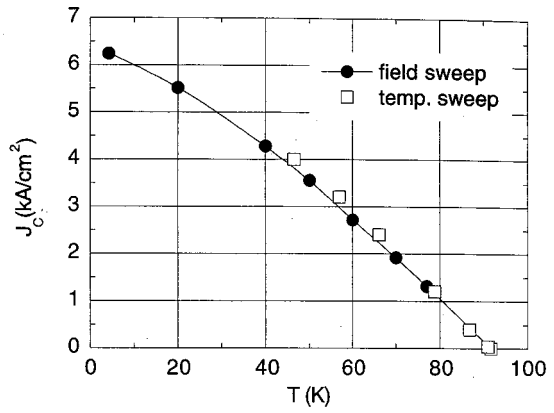

FIG. 4. Critical current density vs temperature for an 11° grain boundary. The critical currents were determined from the temperature and magnetic field where the kinks are observed in Figs. 1 and 3 (see text).

$N=0.67$, agrees very well with the theoretical estimate,[26] $N=1-\pi t/2D=0.66$ for a disk of diameter $D=5$ mm and thickness $t=1.1$ mm. As the field is ramped up, an increasingly larger shielding current is induced in the ring. The kink in M vs H signals the onset of flux penetration into the bore of the ring. For comparison, Fig. 3 also shows 77-K data for the slit ring.

Figure 4 summarizes the results of Figs. 1 and 3. Plotted is the critical current density across the weld joint, J_{cB}, as function of temperature. In both methods, at the kink, the induced current for perfect shielding equals the critical current across the weld. J_{cB} is obtained by dividing this current by the cross section of the ring. In case of a nonuniform distribution of J_{cB}, which can be caused, for example, by a strong-field dependence of J_c, the values quoted here correspond to the average current density in the ring. The results from the temperature and field-dependent measurements show good agreement. A remarkable feature of these results is the almost linear temperature variation $J_{cB}(T)$ near T_c. On an expanded temperature scale this is also visible directly in the temperature dependence of $M(T)$ (see Fig. 2). The temperature dependence of J_{cB} may give information on the superconducting coupling across the boundary. A linear temperature dependence as observed here has been interpreted as a signature of Josephson tunneling in a SIS junction described by the Ambegaokar-Baratoff formalism.[11,19,21] Conversely, a quadratic temperature dependence may be indicative for proximity-coupled SNS junctions.[11,27] However, it is important to note that all the dimensions of the samples studied here are much larger than the Josephson penetration depth $\lambda_J=(\Phi_0/2\pi\mu_0 J_c d)^{1/2}$. Here, d is approximately twice the in-plane penetration depth in the bulk. Thus a complex arrangement of vortices will develop in the boundary (see below) and a description in terms of vortex motion and pinning in a weak link may apply. It has been observed[11,27–29] that a flux-creep controlled critical current can display an approximately linear temperature dependence near T_c.

The penetration of flux into the bore of the ring via a grain boundary can be directly observed employing magneto-optical imaging.[7,22] Imaging studies were done on a second ring cut across the same 11° weld joint as the ring studied in Figs. 1–4. This ring had the same inner and outer diameters as the previous ring, but it was thinned for the magneto-optical studies to a thickness of 0.35 mm. A field sweep $M(H)$ for this ring at 50 K revealed a sharp kink at a field of 60 G (see below in Fig. 7, upper panel, curve marked zfc). The induced shielding current at this field is 24 A, giving a critical current density across the junction (cross section $1.0\times 0.35\,\mathrm{mm}^2$) of 6.8 kA/cm^2 at 50 K.

The left panels of Fig. 5 display a series of magneto-optical images of a small section of the ring containing the artificial grain boundary (at location marked ''joint''). The arrows at the top of the left panel mark the outer and inner peripheries of the ring cross section. The right panels in Fig. 5 are magnetic field scans taken across the ring along the dotted line indicated in the upper left panel (marked ''scan''). The sample was initially cooled in zero field to about 48 K. The field was then increased at constant temperature. The images were taken at various applied fields as specified in the right panels. Red designates the strongest magnetic field, white is intermediate and blue is zero or slightly negative (opposite direction).

At 34 G (top panels) flux is seen to penetrate about 25% of the distance across the boundary. This region of the joint near the sample edge appears to be an excessively weak link with very low J_{cB}. Away from the joint, the ring material is largely field free; the field is concentrated at the outer periphery of the ring. A small negative field is observed at the inner surface of the ring, indicative of supercurrent flowing on the top (and the bottom) surface of the ring. Some field penetration is observable along a line above the weld joint, possibly resulting from small-angle misorientation of subdomains. These types of defects do not affect our measurements as they only minimally reduce the magnetic moment of the ring.

At 45 G (second panels from the top), magnetic flux has penetrated further into the grain boundary, as indicated by the lengthening white line. However, the field profile shows that no flux has yet penetrated into the bore. As the field is further increased, the white line continues to penetrate further into the boundary. A qualitative change is observed in the field profile between 67 and 78 G. Between these two field values, flux has begun to penetrate into the bore. At 78 G, the field scan (right panel) shows there is a positive field in the bore. This is also indicated by the abrupt shift from blue to white coloring in the bore, seen in the left panel. At 90 G, the field in the bore has increased substantially, as revealed in the two bottom panels.

The second weld joint crossing the ring, which is diametrically opposite the one imaged, has a much higher critical current. Complete field penetration into this joint was only observed at fields above 160 G (compared to ~70 G for the joint in Fig. 5). This underscores that substantial variations occur in the properties of the weld joints. The magnetization measurements shown in Figs. 1 and 3 always probe the weakest joint in the ring.

The magneto-optical images show that magnetic flux progressively penetrates the weld joint upon increasing applied field in a manner typical for the development of a critical

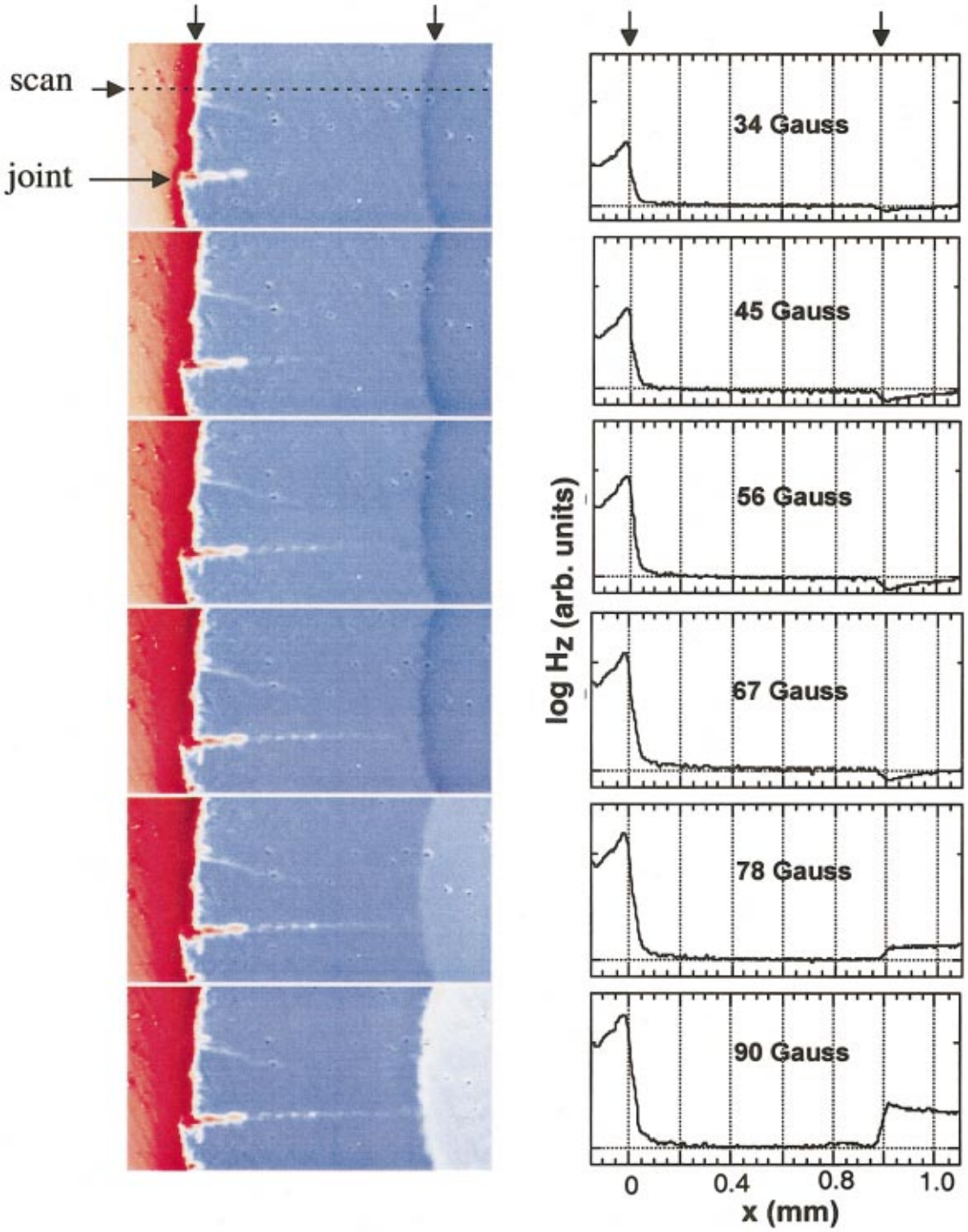

FIG. 5. (Color) Left panels: magneto-optical images at magnetic fields between 34 and 90 G. Right panels: corresponding field scans along dashed line in upper left panel. The magnetic field increases from top to bottom as marked in the right panels. The arrows on top mark the outer and inner peripheries of ring. Arrows on left of top panel indicate position of weld joint and line of field scans (see text). Field scans are on a logarithmic scale.

state. Thus J_{cB} is largely determined by the pinning forces in the grain boundary consistent with the above discussion of the temperature dependence of J_{cB} in terms of vortex creep. Alternatively, it has been argued that for very clean, low pinning boundaries such as produced in multiple seeding processes[13] the critical current density is determined by the self-field at the sample edge.[17] As soon as the field generated by the current flow reaches the penetration field of the boundary vortices will rush all the way to the sample center. The enhanced pinning in welded boundaries studied here is perhaps not surprising since, for the dual-seeded method, the crystallization growth front advances parallel to the grain boundary so that impurity accumulation at the boundary is minimized whereas in the welding process the growth front

moves perpendicular to the boundary. From a practical point of view, the latter boundary is preferred as long as the beneficial effects of Josephson vortex pinning outweigh the negative effects of any loss of superconductivity at the GB due to accumulated impurities.

In conventional transport measurements of the critical current employing I-V characteristics, a voltage criterion must be specified to identify an onset for dissipative behavior. With the methods described here, changes in persistent currents are probed, thus a comparable voltage criterion is not explicitly specified. However, a voltage criterion can be estimated from the time rates of decay of the persistent current. Considering the ring to be a one-turn solenoid, we obtain an induced voltage $V=L(dI/dt)$ where L is the inductance of the ring and dI/dt is the time rate of change of the induced current. The self-inductance of the ring (one-turn solenoid) is approximately $L=2.5\times10^{-8}$ H. At temperatures below the kink temperature (see Fig. 1) we estimate the decay of the current from the observed change in magnetization to be less than 30 μA/s. This corresponds to an induced electric voltage of about 7.5×10^{-13} V induced in the ring. For a (typical) persistent current of 7.5 A, this corresponds to an electrical resistance of about $10^{-13}\,\Omega$. If we assume that all dissipation occurs at the junction the voltage criterion would be around 10^{-12} V across the junction. In reality it is probably much smaller.

High-field measurements (field cooled)

We now consider critical currents measured in the presence of an external magnetic field. For this purpose the ring is cooled in an external field to a predetermined temperature below T_c. The magnetic field is then incrementally increased at a rate of 1.5 G/s and the magnetization is recorded. Results for the ring with the 11° weld joint are shown in Fig. 6 (same ring as used in Figs. 1 and 3). Displayed are magnetization data vs the field-increase ΔH applied after field cooling. The numbers labeling the curves are the cooling fields. The upper panel displays data taken at 77 K, the lower panel at 50 K. The zfc curve for 77 K is the same as that shown in Fig. 3, labeled 77 K. Also shown in both figures is the zfc curve for the slit ring. When the field is initially increased, this added flux is prevented from entering the ring by an induced shielding current that flows around the ring. This initial increase in the magnetization for the field-cooled ring is independent of the cooling field and temperature. It is identical to that in Fig. 3. At the kink in M vs ΔH, the current flowing in the ring first reaches the critical current across the weld. With further increase of the field, additional flux leaks into the bore of the ring. The kinks in M vs ΔH are fairly well defined especially for the 50-K measurements.

Figure 7 displays field-cooled data for two more rings containing weld joints. M vs ΔH data, at 50 K (upper panel), were taken from the same ring (11° grain boundary) which yielded the magneto-optical images of Fig. 5. For this ring the kinks are extremely well defined. Again, the data show that the critical current across the junction (proportional to ΔH at the kink) falls dramatically when small magnetic fields are applied. The lower panel of Fig. 7 displays data,

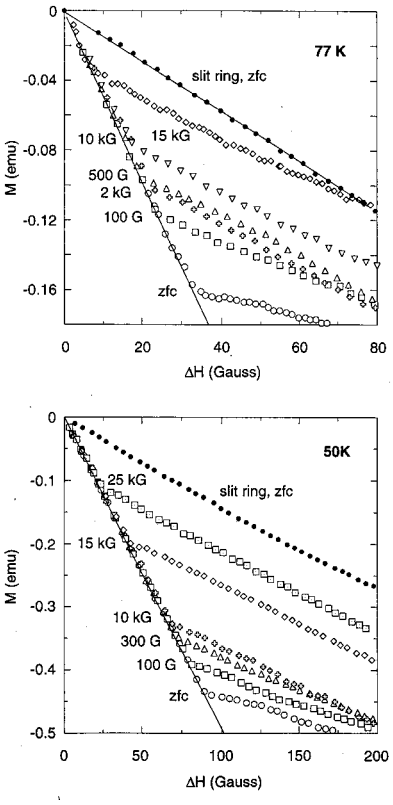

FIG. 6. Field-cooled magnetization for the ring with an 11° boundary. ΔH is the increase in field above the field-cooled value (numbers labeling the curves). Upper panel: at 77 K; lower panel: at 50 K.

taken at 77 K, for a ring with a 6° grain boundary. Here, the kinks in M vs ΔH are not as well defined as in previous examples. The reason for this may be that the critical current across the 6° weld is much higher than for the 11° weld. The kinks therefore occur at higher fields close to or slightly above H_{c1} of the bulk. The flux now also penetrates into the bulk as determined by the bulk critical current density giving rise to a nonlinear M vs H dependence. Nevertheless, the kink can be easily located.

For the low angle boundaries, 3° and 5°, no weak link behavior (i.e., kink in M vs ΔH) was observed. These low angle joints have critical current densities comparable to J_c of the bulk. For these rings, as well as the ring with a 0° weld joint, the critical currents were determined from hysteresis loop measurements, employing the Bean analysis. Figure 8 shows the width of the hysteresis loop ΔM for the ring with the 3° boundary, from which the critical current can be calculated (right scale). To demonstrate that a large shielding current flows through the junction, the ring was slit to prevent circulating currents. The magnetization dropped by about a factor of 3.7 (at 1 T) in good agreement with the theoretical value for this ratio for a homogeneous ring of $(D+d)/(D-d)=4.0$, where $D=$outer, $d=$inner diameter of ring.[6]

Figures 9 and 10 summarize the dependence of the critical current density on grain misorientation and magnetic field. The general features of these results are similar to those re-

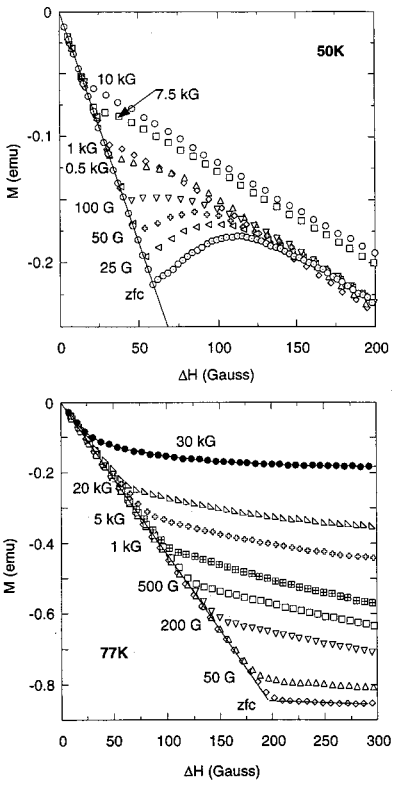

FIG. 7. Determination of the field dependence of the critical current. Upper panel: for the ring used in the magneto-optical imaging (Fig. 5) at 50 K. Lower panel: for a ring with a 6° weld-joint mismatch, at 77 K. For comparison the zero-field-cooled (zfc) runs are also shown. The numbers labeling the curves are the cooling fields.

ported for grain boundaries synthesized with different processes.[11–18] At small misorientation angles (smaller than about 5°) the weld joints carry essentially the same critical current density as the bulk material. The apparent nonmonotonic variation, with angle, at high magnetic fields for the ring with a 0° weld joint, and for the 3 and 5° boundaries (Fig. 9), is attributed to scatter that is usually encountered in

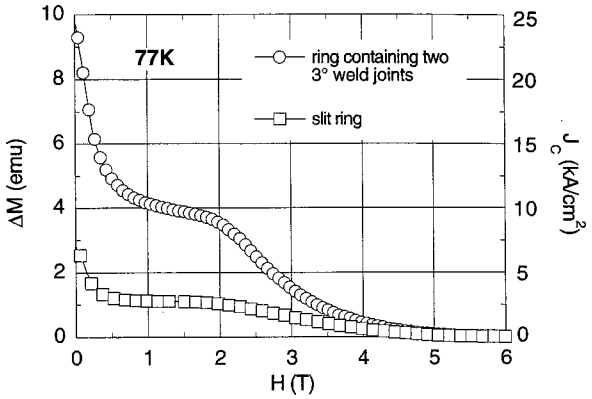

FIG. 8. Width of the hysteresis loop for the ring containing a 3° weld joint. After cutting a slit into the ring the ΔM decreases by about a factor of 3.7 (near $H=1$ T). The right scale gives the critical current densities for the ring.

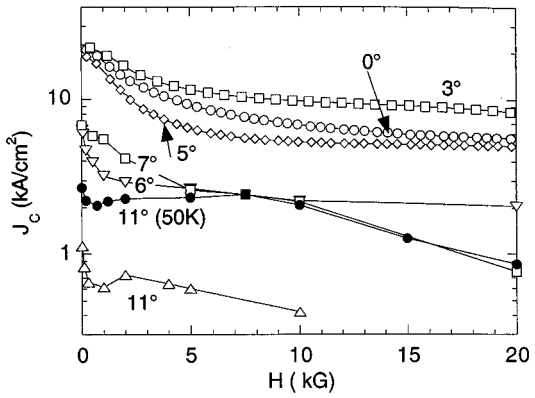

FIG. 9. Critical current density J_c at 77 K for all rings investigated. For the rings with 6, 7, and 11° joints, J_c was determined from the kink in M vs H plots. For the rings with the low angle boundaries, 5, 3, and 0° weld joint, J_c was determined from hysteresis loop measurements employing the Bean model, as in Fig. 8.

such results on technically identical samples. At misorientation angles larger than 5° the critical current density decreases rapidly (Figs. 9 and 10). These high angle boundaries are also characterized by a strong suppression of the critical current density in small applied fields. This effect is more pronounced for larger misorientation angles. This behavior is indicative of the weak link nature of the boundary and the transition from Abrikosov vortices, which exist at small misorientation angles, to Josephson vortices which develop in the junction at high mismatch angles. Qualitatively similar results have been reported for thin-film[18] as well as for bulk[15] boundaries in YBCO. The high angle boundaries, notably the 11° boundary, display a weak peak effect in J_{cB} vs H, similar to that frequently observed in bulk samples. The peak effect is observed in both the 50- and 77-K data. Like J_c measurements in bulk melt textured materials, the peak moves to higher fields as the temperature is reduced.[30] Recently, it has been shown[31,32] that a peak effect in grain boundary critical current density $J_{cB}(H)$ can arise due to the interaction of the grain-boundary vortices with strongly pinned vortices in the neighboring bulk. As the applied field is increased vortices will not only penetrate the boundary but

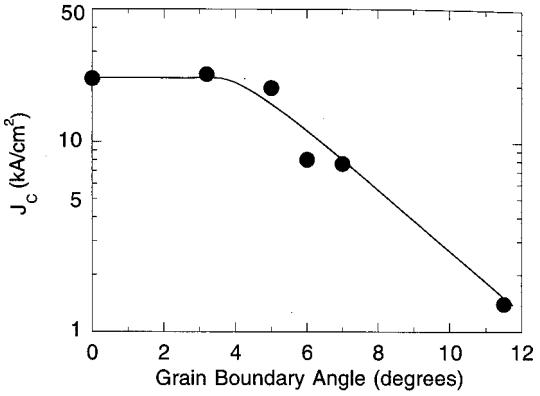

FIG. 10. Critical current in zero field as function of grain-boundary angle.

also to a small extend the neighboring bulk. In a certain field range the repulsive interaction between vortices induces an effective additional pinning potential for the grain-boundary vortices. In even higher fields the grain-boundary vortices are very densely packed and this effect is over come by the overall decrease of J_c with field.

CONCLUSIONS

We have introduced a method to determine critical current densities of grain boundaries utilizing an extremely low-voltage criterion. The method consists of monitoring the persistent currents in ring samples, which contain a grain boundary. The critical current is determined from a sharp kink (an abrupt change in slope) in either the temperature dependence of $M(T)$ at constant magnetic field, or the field dependence of $M(H)$ at constant temperature after initially cooling the ring in zero magnetic field. The method can be extended to determine the critical current as a function of the applied field, by field cooling the rings to low temperatures. We determined the critical current across a series of [001] tilt grain boundaries prepared by welding two melt-textured YBCO pieces at various **ab**-plane mismatch angles. Consistent with prior studies, it is found that grain boundaries, with up to 5° of misorientation, have essentially the same critical current density as bulk YBCO. At higher angles, J_c rapidly declines with increasing mismatch angle. The general behavior of J_{cB} as function of temperature, magnetic field, and misorientation angle is similar to that observed for thin-film grain boundaries except that the absolute value of the critical currents for the melt-textured material is considerably lower.

ACKNOWLEDGMENTS

This research was supported by the U.S. Department of Energy, Basic Energy Science, Materials Science under Contract No. W-31-109-ENG-38.

[1] K. Salama and V. Selvamanickan, Appl. Phys. Lett. **60**, 898 (1992).

[2] K. Kimura, K. Miyamoto, and M. Hashimoto, *Advances in Superconductivity VII* (Springer-Verlag, Tokyo, 1995), p. 681.

[3] M. P. Delmare, H. Walter, B. Brigmann, A. Leeders, and H. C. Freyhardt, Physica C **329**, 257 (2000).

[4] T. Prikhma, W. Gawalek, V. Moshchill, A. Surzhenko, A. Koryuk, D. Litzkendorf, S. Dub, V. Melnikov, A. Plyushchay, N. Sergienko, A. Koval, S. Bokoch, and T. Habisreuther, Physica C **354**, 333 (2001).

[5] W. Lo, D. A. Cardwell, A. D. Bradley, R. A. Doyle, Y. H. Shi, and S. Lloyd, IEEE Trans. Appl. Supercond. **9**, 2042 (1999).

[6] H. Zheng, M. Jiang, R. Nikolova, V. Vlasko-Vlasov, U. Welp, B. W. Veal, and H. Claus, Physica C **309**, 17 (1998).

[7] H. Zheng, M. Jiang, R. Nikolova, U. Welp, A. P. Paulikas, Yi Huang, G. W. Crabtree, and B. W. Veal, Physica C **322**, 1 (1999).

[8] H. Zheng, H. Claus, L. Chen, A. P. Paulikas, B. W. Veal, B. Olsson, A. Koshelev, J. Hull, and G. W. Crabtree, Physica C **350**, 17 (2001).

[9] E. Mendoza, T. Puig, E. Varesi, A. E. Carrillo, J. Plain, and X. Obradors, Physica C **334**, 7 (2000).

[10] B. W. Veal, H. Zheng, H. Claus, L. Chen, A. P. Paulikas, A. Koshelev, and G. W. Crabtree, 2000 International Conference on Superconductivity; Kunibike Messe, Matsue, Shimane, Japan, June 19–22, 2000 (unpublished).

[11] J. Mannhart, P. Chaudhari, D. Dimos, C. C. Tsuei, and T. R. McGuire, Phys. Rev. Lett. **61**, 2476 (1988); D. Dimos, P. Chaudhari, and J. Mannhart, Phys. Rev. B **41**, 4038 (1990).

[12] N. F. Heinig, R. D. Redwing, I. F. Tsu, A. Gurevich, J. E. Nordman, S. E. Babcock, and D. C. Larbalestier, Appl. Phys. Lett. **69**, 577 (1996).

[13] V. R. Todt, X. F. Zhang, D. J. Miller, M. St. Louis-Weber, and V. P. Dravid, Appl. Phys. Lett. **69**, 3746 (1996).

[14] Z. G. Ivanov, P. A. Nilsson, D. Winkler, J. A. Alarco, T. Claeson, E. A. Stepantsov, and A. Ya. Tzalenchuk, Appl. Phys. Lett. **59**, 3030 (1991).

[15] M. B. Field, D. C. Larbalestier, A. Parikh, and K. Salama, Physica C **280**, 221 (1997).

[16] H. Hilgenkamp and J. Mannhart, Appl. Phys. Lett. **73**, 265 (1998).

[17] K. E. Gray, M. B. Field, and D. J. Miller, Phys. Rev. B **58**, 9543 (1998).

[18] N. F. Heinig, R. D. Redwing, J. E. Nordman, and D. C. Larbalestier, Phys. Rev. B **60**, 1409 (1999).

[19] H. Darhmaoui and J. Jung, Phys. Rev. B **53**, 14 621 (1996).

[20] M. Charalambous, R. Koch, A. D. Kent, and W. T. Masselink, Phys. Rev. B **58**, 9510 (1998).

[21] J. Jung, I. Isaac, and M. A-K. Mohamed, Phys. Rev. B **48**, 7526 (1993).

[22] D. T. Verebelyi, C. Cantoni, J. D. Budai, D. K. Christen, H. J. Kim, and J. R. Thompson, Appl Phys. Lett. **78**, 2031 (2001).

[23] U. Welp, D. O. Gunther, G. W. Crabtree, W. Zhong, U. Balachandran, P. Haldar, R. S. Sokolowsky, V. K. Vlasko-Vlasov, and V. I. Nikitenko, Nature (London) **376**, 44 (1995).

[24] E. H. Brandt, Phys. Rev. Lett. **74**, 3025 (1995); E. H. Brandt, Rep. Prog. Phys. **58**, 1465 (1995); G. P. Mikitik and E. H. Brandt, cond-mat/0003388 (unpublished), and references therein.

[25] An alternative way to determine the current flowing in the ring is from the magnetic moment it produces $M = I^*A$ where A is the area of the current loop. This method yields current values about 30–40 % lower than the solenoid formula. The uncertainty here lies in the calibration of the magnetometer which depends on the shape of the sample. For comparing results obtained in different magnetometers we prefer to use the solenoid formula.

[26] J. A. Osborn, Phys. Rev. **11**, 351 (1945).

[27] D. G. Steel, J. D. Hettinger, F. Yuan, D. J. Miller, K. E. Gray, J. H. Kang, and J. Talvacchio, Appl. Phys. Lett. **68**, 120 (1996).

[28] M. Tinkham, Helv. Phys. Acta **61**, 443 (1988).

[29] A. M. Campbell and J. E. Evetts, *Critical Currents in Superconductors* (Taylor & Francis LTD, London, 1972).
[30] A. A. Zhukov, H. Küpfer, G. Perkins, L. F. Cohen, A. D. Caplin, S. A. Klestov, H. Claus, V. I. Voronka, T. Wolf, and H. Wühl, Phys. Rev. B **51**, 12 704 (1995).
[31] A. Gurevich and L. D. Cooley, Phys. Rev. B **50**, 13 563 (1994).
[32] D. Kim, P. Berghuis, M. B. Field, D. J. Miller, K. E. Gray, R. Feenstra, and D. K. Christen, Phys. Rev. B **62**, 12 505 (2000).